Supporting Information

Transition metal dichalcogenide micromotors with programmable photophoretic swarming motion

Víctor de la Asunción-Nadal, Daniel Rojas, Beatriz Jurado-Sánchez,* and Alberto Escarpa*

Experimental Section

Chemicals and Instruments. Tungsten (IV) sulfide (cat. 790583) and N,N-Dimethylformamide (cat. 270547) (Cat. no. R8001) were purchased from Sigma and used without further purification. An ultrasonic processor (Vibra-cell Sonics, VCX 130) was used to exfoliate the commercial material. Optical microscopy images were taken using an inverted optical microscope (Nikon Eclipse Instrument Inc.Ti2-U), coupled with a PCO Panda 4.2bi camera. Samples were irradiated using a D-LEDI (Nikon) LED light source equipped with four intensity-programmable wavelength inputs (385 nm, 475 nm, 550 nm, and 621 nm). Additionally, the light output of each wavelength was measured with a Thorlabs PM100D power meter, resulting in 128.4 mW (385 nm), 82.0 mW (475 nm), 105.4 mW (550 nm), and 117.0 mW (621 nm). TEM images were taken using a Zeiss EM10C microscope. An ALPHA 300AR Raman/AFM microscope (Witec, Germany) was used to collect the Raman spectra and perform the AFM mapping.

Preparation of photophoretic TMD microflakes. Photophoretic TMD microflakes were prepared from commercial tungsten disulfide. 15 mg of the dichalcogenide were weighted in a glass vial, mixed with 20 mL of solvent (DI water or DMF) and sonicated for 2 hours at 80% power (104 W) and 66% duty cycle.

Preparation of magnetic photophoretic Fe_2O_3@WS_2 microflakes. Photophoretic WS_2 microflakes where incubated in a solution containing Fe_2O_3 magnetic microparticles. The obtained particles were sonicated at 6000 RPM for 5 minutes and the supernatant was discarded, and the particles were resuspended in DI water. This step was repeated 3 times. The centrifuged magnetic particles were then separated from the bulk by an external permanent magnet. The supernatant was again removed and the particles that were attracted by the magnet were resuspended in DI water and stored for further use. Prior the use of this particles as light-driven micromotors, they were sonicated again following the steps of the preparation of photophoretic TMD microflakes.

Study of photophoretic capabilities. In a typical experiment, 2 µL of a dispersion containing photophoretic microflakes were placed on a glass slide and irradiated using a xenon arc lamp. The light irradiation was filtered using the required filter cube and focused using a 20x microscope objective. Videos were recorded and analyzed using the NIS Elements AR 3.2 software. To accurately track the velocity of the microflakes, high frame-rate videos were needed, as lower frame rates make them blurry and impossible to track. To this end, we used a high-intensity white illumination light combined with the corresponding filtered excitation light. The application of this white light did not show interaction with the overall motion of the flakes and allowed for the frame capture at low exposure times (24 ms).

Amperometry experiments. The generation of oxidative species was evaluated using a Micrux HVStat potentiostat. A transparent screen-printed indium tin oxide (ITO) electrode manufactured by Dropsens was employed to record the photocurrent at -0.6 V vs Ag reference electrode while the samples were irradiated in the transversal axis. Phosphate-buffered saline was employed as a supporting electrolyte.

Study of photophoretic capabilities in closed well conditions. Experiments were carried out limiting the liquid-air interface to avoid contribution of the Marangoni effect on the motion of the WS_2 light-driven micromotors. The corresponding micromotor solution was introduced in a well of a 96-well plate until the reservoir was filled completely (approx. 300 µL). The plate was then closed with a transparent lid and the motion capabilities were then studied normally.

Supporting Figures

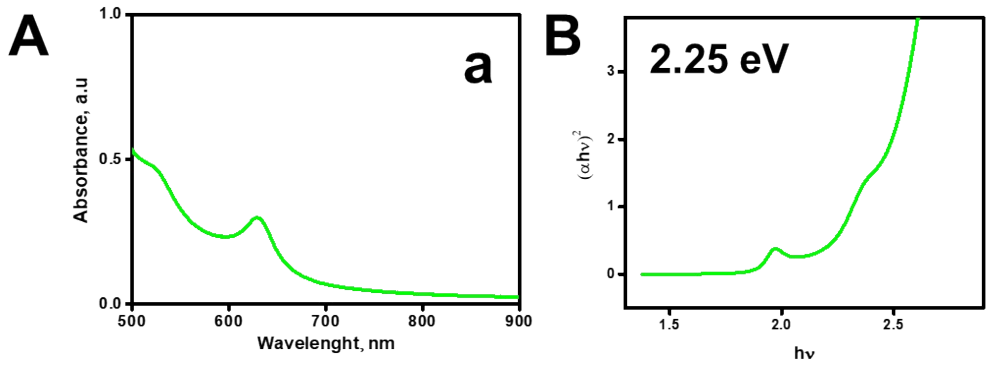

Figure S1. (A) UV-VIS and (B) corresponding TAUC plot of the WS_2 microflakes.

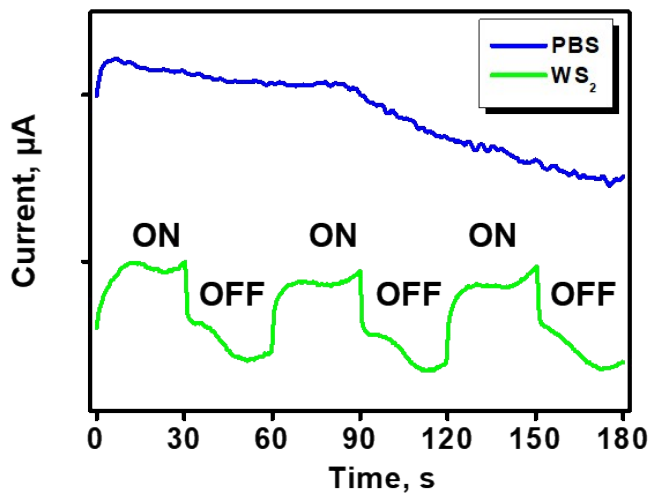

Figure S2. Photocurrent of PBS and WS_2 micromotors in PBS under -0.6 V with intermittent irradiation.

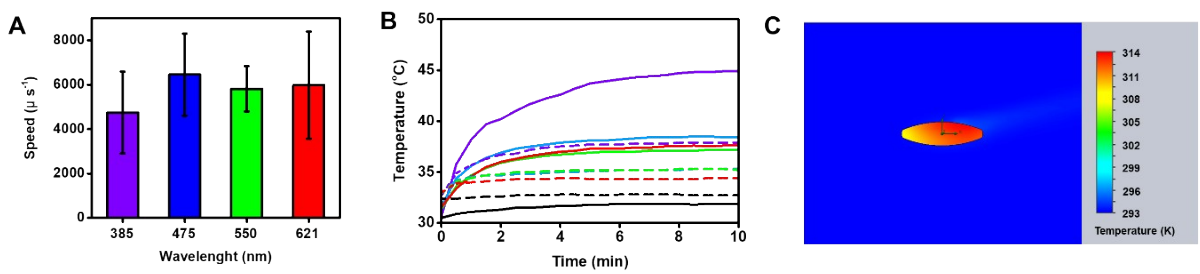

Figure S3. A) Mean speed of photophoretic WS_2 micromotors in DMF. B) Bulk temperature of WS_2 dispersions in DMF (solid lines) and DMF without micromotors (dashed lines) under different 385 nm (violet lines), 475 nm (blue lines), 550 nm (green lines), and 621 nm (red lines). C) Simulation of a single microflake in DMF irradiated in operational conditions.

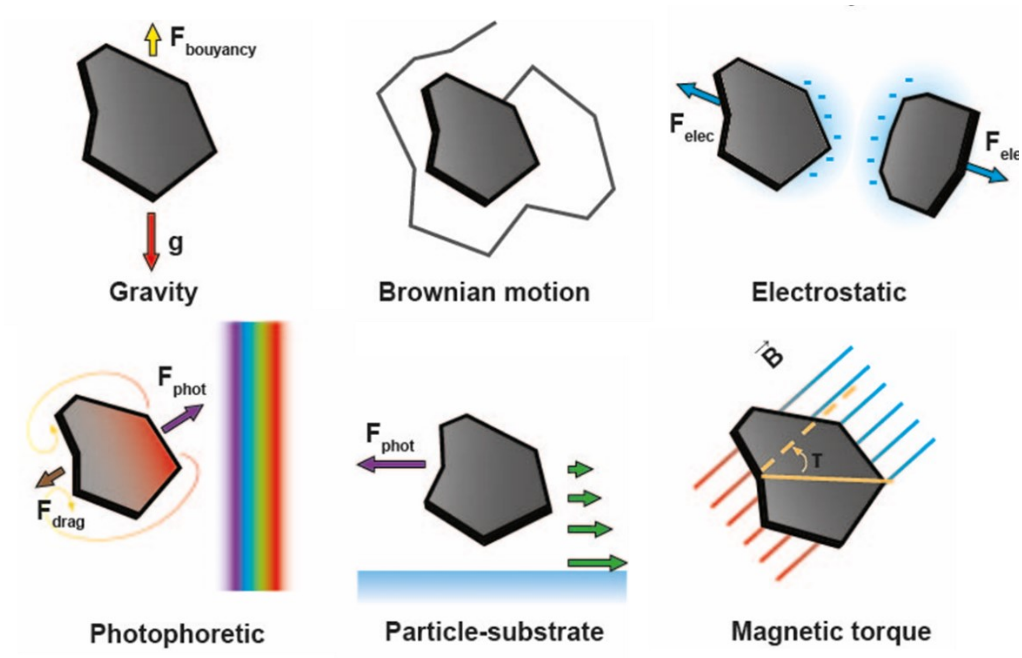

Figure S4. Schematic depiction of the main contributions to the motion of the MoS_2 photophoretic micromotor system.

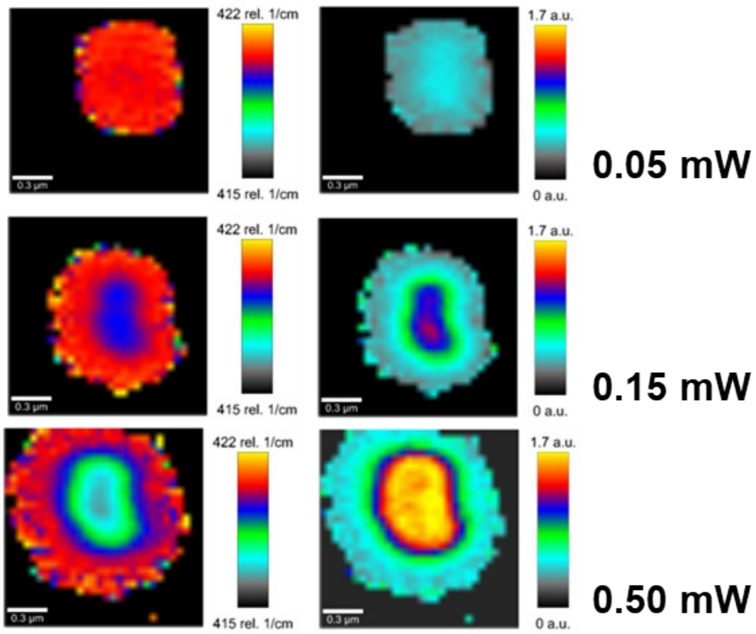

Figure S5. Mapping of Raman shift of the 418 cm^{-1} band (left) and 418 cm^{-1}/352 cm^{-1} amplitude ratio (right) under external irradiation at different irradiation power.

Propulsion mechanism

In order to define the parameters affecting the displacement in the different spatial axes, a non-dimensional depiction of the photophoretic motion in our system was modelled. The main contributions (Schematically depicted in **Figure S4**) need to be defined as follows.

Weight is defined as a downwards acceleration $(w = m{\cdot}g)$ opposed to the buoyancy of the body defined by the Archimedes principle $(F_{bouyancy} = \rho{\cdot}g{\cdot}V)$. Additionally, a random Brownian motion is observed in particles floating on the microscale, it can be statistically estimated. Complementarily, magnetic torque can be observed in magnetic materials in presence of a magnetic field and can be defined as a vector multiplication of the applied field and the magnetic dipole $(\vec{\tau} = \vec{B}\ x\ \vec{M})$. Besides torque, a translational force can be induced in a magnetic gradient as a function of the derivative of the magnetic field magnitude along the vertical axis. Nevertheless, this effect is not observed experimentally, as the magnetic field is applied in the quasiuniform region.

Furthermore, being charged objects, the particles are subject to electrostatic interactions defined by Coulomb's law $(F_{elec} = k\frac{q_1 q_2}{r^2})$, as seen in the corresponding formula, this interaction depends on the magnitude and symbol of the different charges and decreases with the square of the distance between particles.

Moreover, we will define the photophoretic force exerted on the micromotors. As previous reports indicate, this force is a function of the irradiation power, which in our approximation we will relate to the distance to the focal point. Also, as the reports indicate, photophoretic force can induce both trapping and repulsion in the operation axis. Here, we will set the dependencies in an attempt to simulate the observed motion.

Finally, any fluid moving on a surface will slow down on such surface generating a velocity boundary layer which can be defined as a function of the distance between a point in the fluid body and the substrate. Also, electrostatic interactions may appear between the particles and the substrate. Experimentally, two regimes are observed; On one hand, the micromotors display a fast convective motion in the bulk of the fluid. Alternatively, in the close vicinity of the substrate, micromotors display a slow "crawling" motion towards the focal point.

To economize computing power allowing for simulations involving more particles, a series of assumptions and simplifications need to be taken:

- Particles are assumed to be spherical and magnetic torque is not considered.
- All energy inputs are added as a position increment in one of the main axes in each time step in an additive manner.
- Particles will only interact electrostatically with the particles in their vicinity, and inter-particle distance is limited to avoid inconsistencies.

- Gravity and buoyancy will be treated as a single downwards velocity.
- Only two regimes will be considered: Free moving particles in the fluid bulk and substrate-restricted particles. In the latter, interparticle electrostatic interaction will be restricted as particle-substrate interactions are assumed to overcome that contribution.
- Drag force is assumed to have a dependency with the square of velocity on either axis.
- The motion in the vertical and horizontal planes will be illustrated in separate simulations. In the case of the simulation corresponding to the horizontal plane, only the particle-substrate interface will be taken into consideration.

Firstly, a screen with predefined dimensions is generated. Then a list containing a defined number of elements is generated for the position in x and y axes and the positions are designed as a random value for each of the values in the list. Then the position of the particles (obj) is restricted to the boundaries of the screen and gravity-bouyancy (g) is applied as:

objx = objx + **Random value**; objy = objy + **Random value** + **g**

To evaluate the interparticle interactions, every single particle is evaluated against all the other particles. The interparticle distance is then evaluated as the magnitude of the vector subtraction of the origin-coordinate vectors for x and y axis. If the distance is between the predefined limits and the particle is in the bulk fluid region, the angle between particles is evaluated using the atan2 function. The coordinate increment is evaluated as a function of the inverse of distance squared, an electrostatic constant (c_e) that can be set to 1 for electrostatic attraction and -1 for electrostatic repulsion, and a force constant (elec):

$objx_1 = objx_1 + f_{elec,x}(elec,d^2,c_e) \cdot \cos(ang_{pp})$; $objy_1 = objy_1 + f_{elec,y}(elec,d^2,c_e) \cdot \sin(ang_{pp})$

Next, the photophoretic effect was evaluated. Firstly, the particle-focal point distance and angle was evaluated limiting the contribution in the y axis to the bulk region. Then, the photophoretic effect was evaluated obtaining the best match with a linear inverse relationship with the horizontal distance and with the inverse of the square of the vertical distance between the particle and the focal point. In order to correct the contribution of the photothermal effect, a photothermal coefficient was included (c_{ph}). Then the drag force was defined as a function of the speed squared in the corresponding axis times a correction factor (c_{drag}).

$objx_1 = objx_1 + f_{ph,x}(c_{ph},d) \cdot \sin(ang_{pp}) - f_{drag,x}(f_{ph,x}{}^2 \cdot c_{drag})$, $objy_1 = objy_1 + f_{ph,y}(c_{ph},d^2) \cdot \cos(ang_{pp}) - f_{drag,y}(f_{ph,y}{}^2 \cdot c_{drag})$

Hence, by defining simple relationships between the different forces involved in the photophoretic motion of our system, the resulting particle-particle, particle-substrate, and particle-light can be rationalized in a visual way.

Table S1. Relevant examples of reported light-driven micromotors sorted by spectral range, maximum recorded speed, and motion mechanism

Spectral range	Speed ($\mu m\ s^{-1}$)	Propulsion mechanism	Reference
UV	Up to 32 (5 w/o H_2O_2)	Photocatalytic (1% H_2O_2)	[1]
UV	Up to 23	Diffusiophoretic	[2]
UV	Up to 16	Diffusiophoretic	[3]
NIR	Up to 40	Thermophoretic	[4]
UV	Up to 6	Photocatalytic (2% H_2O_2)	[5]
UV	Up to 13	Photocatalytic (1% H_2O_2)	[6]
UV	Up to 5	Photocatalytic (2% H_2O_2)	[7]
UV and VIS	>6000	Photothermal	This work

References

1. X. Peng, M. Urso and M. Pumera, *ACS Nano,* 2022, **16**, 7615-7625.
2. V, Sridhar, F. Podjaski, Y. Alapan, J. Kröger, L. Grunenberg, V. Kishore, B. V. Lotsch and M. Sitti, *Sci. Robot.*, 2022, eabm1421.
3. M. Urso, M. Ussia, F. Novotny and M. Pumera, *Nat. Commun.*, 2022*,* **13**, 1-14.
4. S. Fu, D. Fu, D. Xie, L. Liu, B. Chen, Y. Ye, D. A. Wilson and F. Peng, *Appl. Mater. Today*, 2022, **26**, 101348.
5. P. Mayorga-Burrezo, C. C. Mayorga-Martinez and M. Pumera, *Adv. Funct. Mater.*, 2022, **32**, 2106699.
6. M. Urso, M. Ussia and M. Pumera, *Adv. Funct. Mater.*, 2021, **31**, 2101510.
7. M. Ussia, M. Urso, K. Dolezelikova, H. Michalkova, V. Adam and M. Pumera, *Adv. Funct. Mater.*, 2021, **31**, 2101178.

Supporting Videos

Video S1. Reversible swarming of WS_2 micromotors.

Video S2. Motion and particle trajectories of WS_2, GO and PS beads under UV, green, blue, and red-light irradiation.

Video S3. Magnetic manipulation photophoretic actuation of Fe_2O_3@WS_2 micromotors.

Video S4. WS_2 micromotors in a closed well before and during irradiation at 385 nm.